naturally. (2) The waveguide arises from a higher refractive index in the junction plane. (3) The asymmetry in this dielectric waveguide is sufficiently small to allow propagation of discrete modes. (4) For parameter values characteristic of the GaP p-n junctions studied, only the lowest-order discrete mode of each polarization can propagate. (5) The product of the fractional optical dielectric constant increase and the width over which it extends is independent of bias. (6) The linear electro-optic (Pockels) effect creates a birefringent layer coincident with the junction depletion layer which expands with voltage. (7) Certain anomalies in the phase measurements are best explained as arising from a small quadratic electro-optic (Kerr) effect, though the agreement falls short of a proof of its presence.

Two aspects of this problem need further work. One is the fabrication of diodes at least 1 cm in length from optically and electrically homogeneous crystals. By so doing the intensity of continuum modes, which arise from the satisfaction of boundary conditions at the input surface, will be greatly reduced at the output surface. This should improve the accuracy of both intensity and phase measurements and allow more definitive studies of secondary characteristics such as the Kerr-effect contribution. The second aspect needing further attention is the understanding of the mechanism which creates the higher refractive index inside the p-n junction. The present situation regarding this was summarized at the end of Sec. V.

ACKNOWLEDGMENTS

We wish to thank F. A. Trumbore and C. J. Frosch for growing the crystals, E. Dickten and P. W. Foy for fabricating the diodes, H. F. Tiersten for calculating the effect of the clamping of the junction layer by the bulk crystal, K. F. Rodgers and J. J. Schott for the assistance in measurements, and J. K. Galt, R. C. Miller, and C. D. Thurmond for useful suggestions.

PHYSICAL REVIEW VOLUME 177, NUMBER 3 15 JANUARY 1969

Determination of the Gradient-Elastic Tensors for $A^{III}B^{V}$ Compounds Using Nuclear Acoustic Resonance*

R. K. SUNDFORS
Arthur Holly Compton Laboratory of Physics, Washington University, St. Louis, Missouri 63130
(Received 8 July 1968)

Acoustic waves in crystalline solids can couple energy to nuclear spin systems via the nuclear electric quadrupole interaction. For a known quadrupole moment, measurement of the acoustic attenuation due to this interaction allows the determination of the components of the fourth-order tensor connecting electric field gradients to elastic strains. By the use of nuclear acoustic resonance at 300°K, the magnitudes and relative signs of the gradient-elastic tensor components have been determined for type $A^{III}B^{V}$ semiconducting single crystals at the A and B nuclear positions in InAs, InSb, GaAs, and GaSb and at the B nuclear position in AlSb. The experimental error is $\pm 6\%$ in the measured product of quadrupole moment and gradient-elastic tensor component. Ionic contributions to the electric field gradients alone do not explain the relative signs and magnitudes of the components. A physical model is proposed to separate the ionic and covalent contributions to the measured gradient-elastic tensor components. This model predicts the ratio of the ionic contributions to the tensor components at the same nuclear positions in two different compounds and in the same compound. Such a model can be used to compare the several sets of effective ionic charges that have been proposed for these compounds. The ionic contributions found from this model have magnitudes that can be explained by antishielding coefficients smaller than 220. The covalent contributions at A and B nuclear positions have different magnitudes and different signs.

I. INTRODUCTION

ELASTIC strains have appreciable interaction with the nuclear spin systems in the $A^{III}B^{V}$ semiconducting compounds. In the presence of strains, the cubic symmetry at A and B nuclear positions of the unstrained perfect crystal is destroyed and electric field gradients are created. The electric field gradients interact via the large nuclear electric quadrupole moments with the nuclear spin systems. The over-all interaction between elastic strains and the nuclear spin systems can then be considered to consist of two parts: (i) the coupling between elastic strains and electric field gradients, and (ii) the nuclear electric quadrupole interaction. Our lack of knowledge about (i) is conveniently represented by a fourth-order tensor[1] $\mathbf{S}$ connecting the elastic strain tensor $\boldsymbol{\epsilon}$ to the electric field gradient tensor,

$$\nabla_i\nabla_j V = V_{i,j} = \sum_{k,l} S_{ijkl}\epsilon_{kl} \quad (i,j,k,l = x,y,z). \qquad (1)$$

*This work supported by the National Science Foundation under NSF Grant No. GP-6525.

[1] E. F. Taylor and N. Bloembergen, Phys. Rev. **113**, 431 (1959); E. F. Taylor, Ph.D. thesis, Harvard University, 1958 (unpublished).

This definition of the S tensor is dependent on crystal symmetry but not on any assumed model for the production of electric field gradients.

In this paper, we report the accurate measurement of the S-tensor components in a series of $A^{III}B^{V}$ single crystals. We also consider what the measured S-tensor components indicate about contributions to electric field gradient generation and chemical bonding.

The nonzero S-tensor components can be determined for the $A^{III}B^{V}$ compounds from the symmetry of the tetrahedral T_d group; in the Voigt notation they are S_{11}, S_{12} and S_{44}. Nuclear quadrupole coupling between the elastic strains and a nuclear-spin system can be written[2] in terms of combinations of the two independent constants S_{11}-S_{12} and S_{44}, which we shall call in this paper the S-tensor components.

Measurements of the S-tensor components have been reported in the alkali halides[1,3–7] and in the III-V semiconductors,[8,9] using three different, but related, investigative techniques. One method determines the S-tensor components by observing the quadrupole broadening of an NMR line shape due to an applied static uniaxial stress[7,8] or due to the presence of internal strains from a known concentration of dislocations[3] or impurity atoms[6] in a crystal. The second method is an acoustic saturation experiment[1,9] in which the effect on a nuclear-spin system of an ultrasonic elastic-strain field of known distribution of strain amplitudes at the Larmor frequency or twice the Larmor frequency is measured by a pulse or cw NMR experiment. The third method is nuclear acoustic resonance,[10,11] NAR. In this method the resonant absorption of the energy of acoustic waves by a nuclear-spin system is detected by monitoring the elastic-strain energy in a cw acoustic-attenuation experiment. An advantage of NAR is that the elastic-strain magnitudes do not enter into the determination of the S-tensor components for certain particular directions of acoustic wave propagation and polarization in a cubic crystal. Furthermore, all of the quantities used in the determination of the product of quadrupole moment and the S-tensor component can be determined rather accurately so that the total experimental error in the product is $\pm 6\%$.

In the next section, we present the theoretical relationships between the S-tensor components and the attenuation of acoustic energy by a nuclear-spin system. In Sec. III we discuss the acoustic properties of the samples and the experimental equipment. In Sec. IV there is a discussion of experimental conditions and a tabulation of the measured S-tensor components. In Sec. V the assumptions of a physical model are used to separate the ionic and covalent contributions to the measured S-tensor components. In the final section we summarize the general properties of the experimental S-tensor components and discuss the results of the physical model.

II. THEORY

The nuclear electric quadrupole Hamiltonian can be written

$$\mathcal{H}_Q = \mathbf{Q}:\nabla\mathbf{E}, \tag{2}$$

where $\mathbf{Q}$ is the nuclear electric quadrupole moment tensor and $\nabla\mathbf{E}$ is the electric field gradient tensor at the nuclear position. At high magnetic fields where the quadrupole interaction is much smaller than the splitting of the Zeeman levels, the nonzero matrix elements of $\mathcal{H}_Q$ are[12]

$$(m|\mathcal{H}_Q|m) = A[3m^2 - I(I+1)](\nabla E)_0, \tag{3a}$$

$$(m|\mathcal{H}_Q|m\pm 1) = \mp(6^{1/2}/2)A(2m\pm 1) \times[(I\pm m+1)(I\mp m)]^{1/2}(\nabla E)_{\pm 1}, \tag{3b}$$

$$(m|\mathcal{H}_Q|m\pm 2) = (6^{1/2}/2)A[(I\mp m)(I\mp m-1) \times(I\pm m+1)(I\pm m+2)]^{1/2}(\nabla E)_{\pm 2}, \tag{3c}$$

where $A = eQ/2I(2I-1)$, Q is the nuclear electric quadruple moment, I is the nuclear spin, and m is the nuclear-spin quantum number. If the z axis is taken as the axis of nuclear-spin quantization, the field-gradient elements are[11]

$$(\nabla E)_0 = -(1/2)V_{zz}, \tag{4a}$$

$$(\nabla E)_{\pm 1} = \pm(6^{1/2}/6)(V_{zx} \pm iV_{yz}), \tag{4b}$$

$$(\nabla E)_{\pm 2} = -(6^{1/2}/12)(V_{xx} - V_{yy} \pm 2iV_{xy}). \tag{4c}$$

In the research described in this report, acoustic waves with transverse or longitudinal polarizations are propagated along a [110] direction of a crystal. Using the transformation procedure described by Taylor,[1] we transformed Eq. (1) from (i), a coordinate system with axes along [100], [010], and [001], to (ii), a coordinate system with x axis along [110], y axis along [$\bar{1}$10], and z axis along [001]. We then transformed the electric field gradient tensor from coordinate system (ii) to an x', y', z' coordinate system. The axis of quantization of the magnetic field is taken along z' which is in the ($\bar{1}$10) plane at an angle of θ measured from the x axis; the y and y' axes are identical. Field gradient elements were computed, using Eqs. (4) and transformed electric field gradient tensor components. Equations (5) list the com-

[2] R. J. Harrison and P. L. Sagalyn, Phys. Rev. **128**, 1630 (1962).
[3] E. Otsuka, J. Phys. Soc. Japan **13**, 1155 (1958).
[4] V. V. Lemanov, Zh. Eksperim. i Teor. Fiz. **40**, 775 (1961) [English transl.: Soviet Phys.—JETP **13**, 543 (1961)].
[5] M. Menes and D. I. Bolef, J. Phys. Chem. Solids **19**, 79 (1961).
[6] Y. Fukai, J. Phys. Soc. Japan **19**, 175 (1964).
[7] J. L. Marsh, Ph.D. thesis, Rensselaer Polytechnic Institute, 1966 (unpublished).
[8] R. G. Shulman, B. J. Wyluda, and P. W. Anderson, Phys. Rev. **107**, 953 (1957).
[9] Y. V. Vladimirtsev, V. A. Golenishchev-Kutuzov, N. A. Shamukov, and I. S. Aver'yanov, Fiz. Tverd. Tela **9**, 2426 (1967) [English transl.: Soviet Phys.—Solid State **9**, 1899 (1968)].
[10] D. I. Bolef and M. Menes, Phys. Rev. **114**, 1441 (1959).
[11] D. I. Bolef, *Physical Acoustics* (Academic Press Inc., New York, 1966), Vol. 4A, Chap. 3.
[12] R. V. Pound, Phys. Rev. **79**, 685 (1950).

puted field gradient elements for $\Delta m=\pm 1$ and ± 2 transitions in terms of elastic-tensor strain amplitudes for the following three cases: longitudinal-stress amplitude σ_{xx}, transverse-shear amplitude σ_{xy}, and transverse-shear amplitude σ_{xz}.

$$|(\nabla E)_{1xx}| = (6^{1/2}/12)\sin 2\theta[(S_{11}-S_{12})(\tfrac{1}{2}\epsilon_{xx}+\tfrac{1}{2}\epsilon_{yy}-\epsilon_{zz}) +S_{44}(\epsilon_{xx}-\epsilon_{yy})]$$
$$= (6^{1/2}/12)\sin 2\theta[(S_{11}-S_{12})(\tfrac{1}{2}s_{11}-\tfrac{1}{2}s_{12}) +2S_{44}s_{44}]\sigma_{xx}, \quad (5a)$$

$$|(\nabla E)_{2xx}| = (6^{1/2}/12)[-\cos^2\theta(S_{11}-S_{12})(\tfrac{1}{2}\epsilon_{xx}+\tfrac{1}{2}\epsilon_{yy}-\epsilon_{zz}) +(1+\sin^2\theta)S_{44}(\epsilon_{xx}-\epsilon_{yy})]$$
$$= (6^{1/2}/12)[-\cos^2\theta(S_{11}-S_{12})(\tfrac{1}{2}s_{11}-\tfrac{1}{2}s_{12}) +2(1+\sin^2\theta)S_{44}s_{44}]\sigma_{xx}, \quad (5b)$$

$$|(\nabla E)_{1xy}| = (6^{1/2}/12)\cos\theta(S_{11}-S_{12})\epsilon_{xy}, \quad (5c)$$

$$|(\nabla E)_{2xy}| = (6^{1/2}/12)\sin\theta(S_{11}-S_{12})\epsilon_{xy}, \quad (5d)$$

$$|(\nabla E)_{1xz}| = (6^{1/2}/6)\cos 2\theta S_{44}\epsilon_{xz}, \quad (5e)$$

$$|(\nabla E)_{2xz}| = (6^{1/2}/12)\sin 2\theta S_{44}\epsilon_{xz}. \quad (5f)$$

In Eqs. (5a) and (5b), the elastic-tensor compliances are s_{11}, s_{12}, and s_{44}. The acoustic strain waves whose amplitudes are ϵ_{xx} have longitudinal polarizations and those whose amplitudes are ϵ_{xy} or ϵ_{xz} have transverse polarizations.

In NAR, the relevant experimental quantity related to the S-tensor components is the acoustic attenuation constant for absorption of energy by a nuclear-spin system, α_n. An attenuation constant is defined as equal to the power absorbed per unit volume P_n divided by two times the incident power per unit area P_0 or

$$\alpha_n \equiv P_n/2P_0. \quad (6)$$

The incident acoustic power per unit area is

$$P_0=\tfrac{1}{2}v\sum_{i,j,k,l} c_{ijkl}\epsilon_{ij}\epsilon_{kl}, \quad (7)$$

where c_{ijkl} are the elastic stiffness constants and v is the velocity of the acoustic wave. The power absorbed by the nuclear-spin system per unit volume is[13]

$$P_n=\frac{N}{(2I+1)}\frac{(h\nu)^2}{kT}\sum_m W_{mm'}, \quad (8)$$

where N is the number of nuclei per unit volume participating in the absorption of elastic energy, ν is the frequency of the elastic wave, and $W_{mm'}$ is the transition probability from the spin state m to the spin state m'. For a first-order time-dependent sinusoidal perturbation, we have

$$W_{mm'} = (1/4\hbar^2)|(m|\mathcal{H}_Q|m')|^2 g(\nu)$$
$$= (3/8\hbar^2)A^2F(I)^2(\nabla E)^2 g(\nu), \quad (9)$$

[13] A. Abragam, *The Principles of Nuclear Magnetism* (Oxford University Press, London, 1961).

TABLE I. Experimental $A^{III}B^{V}$ samples with physical properties determined by the supplier.

Compound	Type	Carrier concentration (cm^{-3})	Mobility (cm^2/V sec)	Resistivity (Ω cm)	Etch-pit density (cm^{-2})
InAs[a]	N	1.4×10^{16}	18,200	0.024	1100
InSb[a]	P	1.5×10^{16}[c]	4,500[c]	0.112[c]	100
GaAs[a]	N	1.4×10^{16}	3,800	0.0115	1200
GaSb[a]	P	1.7×10^{17}	570	0.066	5000
AlSb[b]	P	1.8×10^{16}	265	1.27	...

[a] Supplied by Monsanto Chemical Co.
[b] Obtained from Bell and Howell Research Laboratories.
[c] These values were determined at 78°K, the remainder at 300°K.

where $g(\nu)$ is a normalized line shape function and $F(I)$ is a spin factor given in Eqs. (10).

$$F(I)_{\pm 1}=(2m\pm 1)[(I\pm m+1)(I\mp m)]^{1/2}, \quad (10a)$$

$$F(I)_{\pm 2}=[(I\mp m)(I\mp m-1) \times(I\pm m+1)(I\pm m+2)]^{1/2}. \quad (10b)$$

By substitution of Eqs. (5), and (7)–(10) into Eq. (6), it is easily shown that α_n is independent of the transverse strains and can be written in terms of accurately known physical quantities times the square of the product of the quadrupole moment and the S-tensor component. We show in Eqs. (11) the attenuation for transverse acoustic wave propagation.

$$\alpha_{n1xy}=CB_1Q^2(S_{11}-S_{12})^2\cos^2\theta, \quad (11a)$$

$$\alpha_{n2xy}=CB_2Q^2(S_{11}-S_{12})^2\sin^2\theta, \quad (11b)$$

$$\alpha_{n1xz}=4CB_1(QS_{44}\cos 2\theta)^2, \quad (11c)$$

$$\alpha_{n2xz}=CB_2(QS_{44}\sin 2\theta)^2, \quad (11d)$$

where

$$B_1=\Sigma_m F(I)^2_{\pm 1},$$
$$B_2=\Sigma_m F(I)^2_{\pm 2},$$
$$C=\frac{\pi^2}{16(2I)^2(2I-1)^2(2I+1)}\frac{N\nu^2e^2g(\nu)}{\rho v^3kT},$$

and ρ is the crystal density.

III. EXPERIMENTAL APPARATUS AND PROCEDURES

Some of the physical properties of the $A^{III}B^{V}$ single crystals used in this experiment are shown in Table I. All of the samples are intrinsic except for InSb, which has a Ge dopant at 1.5×10^{16} cm^{-3}. For each crystal, a (110) face was determined, using x-ray-diffractometer techniques to within $\pm 10'$ of arc. We prepared each crystal with a pair of flat and parallel (110) faces of approximately 0.6 in. diam. The flatness of these faces was measured to be within one-half wavelength for Hg light. The difference in perpendicular distance between the faces at different points on the faces was measured to be smaller than 50 μin.

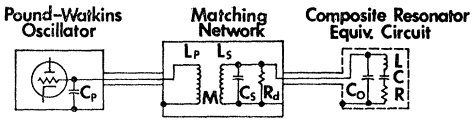

FIG. 1. The matching network between composite resonator and marginal oscillator.

We used either 8 or 10 MHz AT- or X-cut fine-ground quartz transducers with a coaxial plating configuration. The diameter of the radiating area of the transducers was 0.410 in. Polarizations of the AT-cut transducers were oriented to within ± 1 deg of either a [001] or a [$\bar{1}$10] direction. For both X- and AT-cut transducers for these room-temperature experiments, we used pure Canada balsam, applied at 300°F, as a bond. Such bonds were about 50 μin. thick, and the acoustic properties of the transducer, bond, and crystal combination were reproducible. This combination of transducer, bond, and crystal is called the composite resonator.

Within the bandpass of approximately 1 MHz of the fundamental frequency of the loaded-quartz transducer, a number of standing-wave or mechanical resonances occur when the transducer is driven with an rf voltage. The peaks of the mechanical resonances occur when some integer times the wavelength of the acoustic wave in the crystal is twice the crystal length. The mechanical resonances of such a composite resonator can be monitored with swept-frequency techniques and more accurately with an rf bridge such as the Hewlett-Packard model 250A RX meter.

The real part of the electrical response of the loaded transducer is the inverse rf parallel resistance. For mechanical resonances near the center of the fundamental frequency band of the loaded transducer, the inverse rf parallel resistance of the $A^{III}B^{V}$ compound composite resonators agreed with a Lorentz line-shape function when measured as a function of frequency to within an experimental error of $\pm 1\%$. Such a mechanical resonance shape is predicted by representing the composite resonator by a series RLC circuit[14] or from a more detailed analysis.[15] The frequency width of the Lorentz-shape mechanical resonances at half-maximum amplitudes $\Delta\nu$ gave quality factors $\nu/\Delta\nu$ between 10^4 and 10^5 for each of the samples. The parallel rf resistances of the mechanical resonance peaks were usually less than 1000 Ω. The quality factor of a Lorentz line-shape function can be related to an attenuation by the relationship[16]

$$\alpha = \frac{\pi\nu}{v}\frac{\Delta\nu}{\nu}. \tag{12}$$

We measured phase velocities v for each propagation direction and polarization using a cw technique.[16] These measured velocities agreed within an experimental error of less than $\pm 0.5\%$ with those velocities computed from the published values[17] of sample density and sample stiffness constants for 300°K.

Absorption of acoustic energy in the composite resonator is accompanied by a decrease in the quality factor and an increase in the rf parallel resistance at the center of a mechanical resonance. Since the changes in quality factor or acoustic attenuation due to absorption of energy by a nuclear-spin system are very small ($\alpha_n \approx 10^{-5}$–10^{-9} cm^{-1}), we can relate the change in parallel resistance to the change in attenuation by

$$\Delta R = (R/\alpha)\Delta\alpha = (R/\alpha)\alpha_n. \tag{13}$$

In the actual NAR experiment, we placed a double-tuned parallel resonance circuit, shown in Fig. 1, between the composite resonator and a marginal oscillator. The significance of C_0 and R_d in Fig. 1 is discussed by Bolef and Menes.[10] The purpose of the double-tuned resonance circuit is to provide impedance matching between composite resonator and the marginal oscillator and to invert the rf impedance at the center of a mechanical resonance. In this NAR experiment, we "locked" the marginal oscillator, which is a Pound-Knight-Watkins oscillator,[18] to one of the mechanical resonance peaks. A magnetic field was adjusted to give the Larmor condition for $\Delta m = \pm 1$ or ± 2 nuclear-spin transitions for the frequency of the mechanical resonance. The conductance change ΔG at the grid of the oscillator tube of the marginal oscillator due to the absorption of energy by the nuclear-spin system can be written[10]

$$\Delta G = \frac{k^2}{(2\pi)^2\nu^2 L_P L_S}\left(\frac{R_d}{R_d+R}\right)^2 \frac{Rv}{\Delta\nu\pi}\alpha_n, \tag{14}$$

where k is the coupling coefficient for the double-tuned resonance circuit and the other quantities are defined by Fig. 1.

The remainder of the electronic circuit was a conventional cw NMR spectrometer with field modulation frequency at 100 Hz. The modulation field amplitude was calibrated to within a $\pm 1\%$ experimental error. We also used phase-sensitive detection and a calibrator network.[10] This calibrator network was characterized by an af signal, whose amplitude was determined to within a $\pm 2\%$ experimental error. The calibrator signal was introduced at the grid of the oscillator tube of the marginal oscillator. The change of conductance at the grid of the oscillator tube of the marginal oscillator can be written as the product of accurately determined quantities, multiplying the square of the S-tensor component and the square of the quadrupole moment by substituting Eqs. (5)–(10) into Eq. (14).

We found experimentally that the values of S-tensor components, determined for different mechanical reso-

[14] T. F. Heuter and R. H. Bolt, *Sonics* (John Wiley & Sons, Inc., New York, 1955) Chap. 4, p. 99.
[15] J. G. Miller and D. I. Bolef, J. Appl. Phys. **39**, (1968).
[16] D. I. Bolef and J. deKlerk, Trans. IEEE **UE-10**, 19 (1963).
[17] G. Simons, J. Grad. Res. Center **34**, Nos. 1 and 2 (1965).
[18] G. D. Watkins, Ph.D. thesis, Harvard, 1952 (unpublished).

nances of the same composite resonator, did agree within a $\pm 3\%$ experimental error as long as the mechanical resonances were Lorentz line-shape functions and were near the center of the loaded transducer response. Reproducibility of the components of the S tensors for a given crystal for different bonds, different transducers, and different monitoring equipment was within $\pm 5\%$. We conclude from the last two statements that acoustic losses in the transducer bond and transducer are negligible compared to acoustic losses in the $A^{III}B^{V}$ samples. Also we conclude that we are capable of measuring accurately and reproducibly the absorption of energy by the nuclear-spin systems in these samples.

IV. EXPERIMENTAL RESULTS

We observed the NAR transitions shown in Table II at a temperature of 300°K and at frequencies of 8 or 10 MHz by using acoustic waves propagating in a [110] direction with transverse polarizations in the [001] or [$\bar{1}$10] directions. Also listed in Table II are the nuclear spins and the nuclear electric quadrupole moments without shielding corrections. The Al^{27} NAR was not observed, probably because of a combination of a low signal-to-noise ratio and saturation. We observed NAR of Ga^{71} and In^{113}, but the signal amplitudes were too small to be useful. NAR signal-to-noise ratios of greater than 30:1 were observed for In^{115}, Sb^{121}, Sb^{123}, and As^{75} with the following experimental conditions: (i) the modulation field amplitude adjusted to be equal to one-half of the linewidth, (ii) a 10-sec time constant, and (iii) the axis of magnetic field quantization along a [100] direction. The Ga^{69} signal-to-noise ratio was 5:1 for the same experimental conditions.

We determined the saturation levels for each of the nuclear-spin systems and adjusted operating levels for strain amplitudes in order to allow observation of more than 99% of the unsaturated NAR amplitude. The NAR linewidths and line shapes were measured and were found to vary with the direction of the axis of quantization.[19] For the axis of quantization of the nuclear-spin system along some cubic axis, such as a [001] direction, the NAR line shapes for the nuclear-spin systems in each of the samples are Gaussian functions, and the effects of quadrupole broadening are small compared to the line broadening from the indirect spin-spin interaction.[20] We therefore believe that all nuclear spins per unit volume of a particular spin species contribute to the NAR line shape when the axis of quantization is along a [001] direction.

We found that the experimental S-tensor components measured at the Sb^{121} and Sb^{123} nuclear positions had the same values within a $\pm 3\%$ experimental error in the three compounds InSb, GaSb, and AlSb. This measurement indicates that the coupling between elastic strains and nuclear-spin systems is indeed via the nuclear electric quadrupole interaction. Further confirmation of the coupling by the quadrupole interaction was the observation that the experimental NAR nuclear attenuation constants agreed with the expressions developed in Sec. II. The dependence of the experimental α_n on the angle between the axis of quantization and the [110] direction is that given by the squares of the field-gradient expressions of Eqs. (5). Furthermore, $\Delta m = \pm 1$ or ± 2 transitions give the same value for a particular S-tensor component within a $\pm 3\%$ experimental error.

By using acoustic waves propagating in the [110] direction of each crystal with transverse polarizations either in the [001] or [$\bar{1}$10] directions, we measured the absolute magnitude of the product of the quadrupole moment times the S-tensor component at each of the A and B nuclear positions in InAs, GaAs, InSb, and GaSb and at the B nuclear position in AlSb. These measurements are shown in Table III. The experimental error given to this product is $\pm 6\%$ and the reproducibility of the measurement is within $\pm 5\%$ as noted in Sec. III.

By using longitudinal acoustic waves propagating in the [110] direction and observing the NAR for $\Delta m = \pm 2$ transitions for each of the nuclear spin systems in Table II, we determined the relative signs of $S_{11}-S_{12}$ and S_{44} at the A and B nuclear position in each compound except

TABLE II. Observed NAR transitions and nuclear properties.

Compound	Nucleus	Transition observed, $\Delta m = \pm$	I	Q (10^{-24} cm^2)
InAs	In^{115}	1,2	9/2	0.834±0.001[a]
	As^{75}	1,2	3/2	0.32 ±0.05[b]
InSb	In^{115}	1,2	9/2	0.834±0.001[a]
	Sb^{121}	1,2	5/2	0.53 ±0.08[c]
	Sb^{123}	2	7/2	0.68 ±0.10[c]
GaAs	Ga^{69}	1,2	3/2	0.190±0.001[a]
	As^{75}	1,2	3/2	0.32 ±0.05[b]
GaSb	Ga^{69}	1,2	3/2	0.190±0.001[a]
	Sb^{121}	1,2	5/2	0.53 ±0.08[c]
	Sb^{123}	2	7/2	0.68 ±0.10[c]
AlSb	Sb^{121}	1,2	5/2	0.53 ±0.08[c]
	Sb^{123}	2	7/2	0.68 ±0.10[c]

[a] G. F. Koster, Phys. Rev. **86**, 148 (1952).
[b] K. Murakawa, Phys. Rev. **110**, 393 (1958).
[c] K. Murakawa, Phys. Rev. **100**, 1369 (1955).

TABLE III. Measured products of quadrupole moment and S-tensor component (in units of 10^{-9} statcoulomb cm^{-1}). The experimental uncertainty is $\pm 6\%$ in these values.

Compound	Nucleus	$\lvert QS_{44}\rvert$	$\lvert Q(S_{11}-S_{12})\rvert$
InAs	In^{115}	8.3	23.5
	As^{75}	6.8	6.1
InSb	In^{115}	9.8	18.4
	Sb^{121}	17.7	12.4
GaAs	Ga^{69}	1.78	2.64
	As^{75}	7.0	5.4
GaSb	Ga^{69}	2.05	1.85
	Sb^{121}	18.0	10.3
AlSb	Sb^{123}	19.3	15.0

[19] R. K. Sundfors (to be published).
[20] R. G. Shulman, J. M. Mays, and W. D. McCall, Phys. Rev. **100**, 692 (1955).

TABLE IV. Measured S-tensor components (in units of 10^{15} statcoulomb cm^{-3}). The experimental uncertainty is $\pm 6\%$ for In and Ga values and $\pm 20\%$ for As and Sb values.

Compound	Nucleus	S_{44}	$S_{11}-S_{12}$	$2S_{44}/(S_{11}-S_{12})$
InAs	In	$\mp$ 9.9	$\pm$28.2	-0.70
	As	$\pm$21.2	$\pm$19.1	$+2.2$
InSb	In	$\mp$11.7	$\pm$22.0	-1.1
	Sb	$\pm$33.3	$\pm$23.5	$+2.8$
GaAs	Ga	$\mp$ 9.3	$\pm$13.9	-1.4
	As	$\pm$21.9	$\pm$17.0	$+2.6$
GaSb	Ga	$\mp$10.8	$\pm$ 9.8	-2.2
	Sb	$\pm$33.9	$\pm$19.5	$+3.5$
AlSb	Sb	$\pm$28.5	$\pm$22.0	$+2.6$

AlSb. This determination was accomplished by comparing the observed angular dependence of the NAR transition probability with that computed using Eq. (5b). The elastic compliance expressions in Eqs. (5a) and (5b), $\frac{1}{2}(s_{11}-s_{12})$ and s_{44}, can be shown from tabulations of the elastic compliances for these compounds[17] to be both positive. The results of the measurements are that $S_{11}-S_{12}$ and S_{44} have opposite signs at the A nuclear positions in InAs, InSb, GaAs, and GaSb, and identical signs at the B nuclear positions in all five compounds.

From the quadrupole moments of Table II and the products of the quadrupole moment times the S-tensor component of Table III, the S-tensor components are computed. The magnitudes and relative signs of $S_{11}-S_{12}$ and S_{44} and the isotropy factor for field gradients[2] $2S_{44}/(S_{11}-S_{12})$ are given in Table IV. The absolute errors of $S_{11}-S_{12}$ and S_{44} are the sums of the error in the quadrupole moment and the error in the measured product of quadrupole moment and S-tensor component. Therefore, the total uncertainty is $\pm 6\%$ at the In and Ga nuclear positions and $\pm 20\%$ at As and Sb nuclear positions.

The experimental S-tensor components of Table IV can be compared with three other experimental NMR investigations of the S-tensor components at 78°K. Recent static strain experiments[21] measure the same S-tensor components that we present in Table IV. These experiments of Bogdanov and Lemanov[21] yield values of the S-tensor components which disagree with those of Table IV except for the S-tensor components of InSb. This static strain experiment also measures S-tensor components which differ by as much as two orders of magnitude at the same nuclear position in different compounds. However, the results of Table IV indicate that the S-tensor components at the same nuclear position in different compounds are approximately equal. Similar electric field gradients are to be expected at the same nuclear position in different $A^{III}B^{V}$ compounds, because these compounds have similar lattice constants and are believed to have similar chemical bonding.[22]

TABLE V. Comparison of measured S-tensor components of In^{115} Sb.

	Static Strain[a]	Saturation[b]	Static Strain[c]	Table IV
S_{44} (10^{15} statcoulomb cm^{-3})	$\pm$10.2$\pm$2.0		$\pm$ 7$\pm$2	$\pm$11.7$\pm$0.7
$(S_{11}-S_{12})$ (10^{15} statcoulomb cm^{-3})	$\mp$15.0$\pm$3.0	18.0	$\mp$15$\pm$5	$\mp$22.0$\pm$1.3

[a] Reference 8. [b] Reference 9. [c] Reference 21.

In Table V, we compare our measured values of the S-tensor components at the In^{115} nuclear position in InSb at 300°K with the first static strain measurement,[8] the Bogdanov and Lemanov experiment,[21] and an ultrasonic saturation measurement,[9] all at 78°K. These 78°K measurements were rewritten in terms of $S_{11}-S_{12}$ and S_{44}, and the value of the In^{115} quadrupole moment of Table II was used. From Table V we find agreement within experimental error between our measured value of S_{44} and the static-strain experimental value[8]. We also find agreement between the relative signs of the two S-tensor components determined in Table IV and by the static-strain methods.[8,21] Our measured value of $S_{11}-S_{12}$ at 300°K also agrees with the static strain[21] and the saturation values at 78°K, if an experimental error of at least $\pm 15\%$ is attributed to the saturation value.

The following general observations can be made about the experimental S-tensor components by referring to Table IV.

(1) The values of S_{44} measured at the As nuclear positions are approximately the same for InAs and GaAs. The values of S_{44} measured at the Sb nuclear positions are approximately the same for InSb and GaSb but smaller for AlSb. The values of S_{44} at the As nuclear positions are approximately 65% of the values of S_{44} at the Sb nuclear positions in the four compounds InAs, InSb, GaAs, and GaSb.

(2) At an In or Ga nuclear position, the values of S_{44} increase by approximately 20% when the B atom changes from As to Sb.

(3) At the B nuclear positions in the five compounds, the values of $S_{11}-S_{12}$ (in units of 10^{15} statcoulomb cm^{-3}) vary between 17 and 24. At the A nuclear positions for the compounds ordered in the sequence InAs, InSb, GaAs, and GaSb, the values of $S_{11}-S_{12}$ (in units of 10^{15} statcoulomb cm^{-3}) decrease from 28 to 9.8. The isotropy factors at the A nuclear positions increase in this same order.

V. S-TENSOR-COMPONENT CONTRIBUTIONS

The measured S-tensor components in Table IV can be analyzed by comparing them with magnitudes from

[21] V. L. Bogdanov and V. V. Lemanov, Fiz. Tverd. Tela **10**, 212 (1967) [English transl.: Soviet Phys.—Solid State **10**, 159 (1968)].

[22] O. Madelung, *Physics of III-V Compounds* (John Wiley & Sons, Inc., New York, 1964), Chap. 2.

theoretical estimates of ionic and covalent contributions to the electric field gradients. Such a procedure has been used to predict the magnitudes of measured S-tensor components in the alkali halides.[6,7] However, in the $A^{III}B^{V}$ compounds, such an analysis is made even more difficult by the expected[22] large amount of covalent character in the partially ionic, partially covalent chemical bond. Several theoretical estimates of the ionicity of the chemical bond and of the related quantity, the effective ionic charge, have been proposed[23–26] for the $A^{III}B^{V}$ compounds. The effective ionic charge is defined to be the actual ion charge shielded by the valence electrons in the chemical bond.

We propose a simple model to separate the contributions to the S-tensor components which we call ionic and covalent. Because of the uncertainty about the fraction of ionicity and covalency in the chemical bond of the $A^{III}B^{V}$ semiconductors, the model uses, for example, not the magnitudes of a given set of effective ionic charges, but the ratios of the effective ionic charges between compounds. The assumptions of the model are as follows: (i) Each measured S-tensor component can be written as the sum of a point-charge ionic contribution and a covalent contribution due to the valence electron configuration including the chemical bond. We write

$$S_{44}=S_{44}{}^{i}+S_{44}{}^{c}, \tag{15a}$$

$$S_{11}-S_{12}=(S_{11}-S_{12})^{i}+(S_{11}-S_{12})^{c}, \tag{15b}$$

where i and c denote ionic and covalent contributions, respectively. (ii) The ionic point-charge model can be used to give the ratio of $(S_{11}-S_{12})^{i}/S_{44}{}^{i}$ at the same nuclear position in the same compound. The ionic model and one set of effective ionic charges can give the ratio of $S_{44}{}^{i}$ at the same nuclear positions in two different compounds. (iii) At the same nuclear positions in two different compounds, the ratio of the $(S_{11}-S_{12})^{c}$ components is equal to the ratio of the $S_{44}{}^{c}$ components.

With these assumptions, it is possible to solve the four equations (16), which use, for example, the measured S-tensor components from Table IV at the Sb nuclear positions in InSb and GaSb, compounds 1 and 2, respectively:

$$33.3=S_{44}{}^{i1}+S_{44}{}^{c1}, \tag{16a}$$

$$33.9=S_{44}{}^{i2}+S_{44}{}^{c2}, \tag{16b}$$

$$23.5=(S_{11}-S_{12})^{i1}+(S_{11}-S_{12})^{c1}, \tag{16c}$$

$$19.5=(S_{11}-S_{12})^{i2}+(S_{11}-S_{12})^{c2}. \tag{16d}$$

In the following paragraphs, we discuss the ionic point-charge model, the covalent contributions, and the application of the model.

[23] C. A. Coulsen, L. B. Redei, D. Stocker, Proc. Roy. Soc. (London) **270**, 357 (1962).
[24] J. B. Suchet, J. Phys. Chem. Solids **21**, 156 (1961).
[25] F. Bailly, J. Phys. (Paris) **27**, 335 (1966).
[26] N. N. Sirota, *Chemical Bonds in Semiconductors and Solids* (Consultants Bureau Enterprises, Inc., New York, 1967).

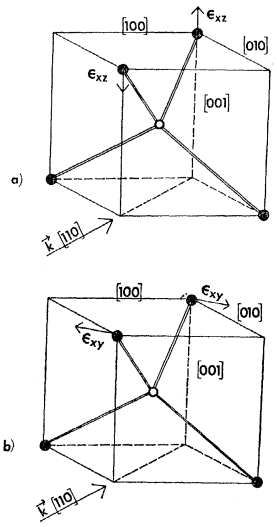

FIG. 2. Nearest-neighbor displacements relative to the center atom: (a) transverse ϵ_{xz} strains which measure S_{44}, (b) transverse ϵ_{xy} strains which measure $S_{11}-S_{12}$.

A. Ionic Model

In order to determine the ionic contributions to the S-tensor components, we consider a point-charge ionic model and calculate the field gradients for the two different elastic strains which are used to measure $S_{11}-S_{12}$ and S_{44}. The wavelengths of the acoustic waves at 10 MHz are of the order of 10^{-2} cm, while the nearest-neighbor distances in the $A^{III}B^{V}$ compounds are of the order of 10^{-8} cm. Therefore, it is a good approximation that the transverse strains, relative to a particular A or B nuclear position, vary linearly with increasing distance to neighboring shells of atoms which produce the ionic field gradients. In terms of the coordinate system defined in Sec. II, with an A nucleus at the origin, the nearest-neighbor strains relative to the A nucleus are shown in Fig. 2. For the ionic model, we replace each neighboring atom by a point charge with charge magnitude equal to an effective ionic charge. To account for the effects on the electrons of the A atom by field gradients external to the A atom and by the nuclear quadrupole moment of the A nucleus, we introduce into the ionic model an antishielding coefficient,[27] $(1-\gamma_\infty)$. The ionic field gradient expressions for V_{xz} and V_{xy} can be written for the A nuclear position as

$$V_{xz}{}^{i}=(+2.9)(1-\gamma_\infty)(e^*/a^3)\epsilon_{xz}=S_{44}{}^{i}\epsilon_{xz}, \tag{17a}$$

$$V_{xy}{}^{i}=(-6.7)(1-\gamma_\infty)(e^*/a^3)\epsilon_{xy}=\tfrac{1}{2}(S_{11}-S_{12})^{i}\epsilon_{xy}, \tag{17b}$$

where e^* is the effective ionic charge, a is the nearest-neighbor distance, and the numerical factors are computed for ϵ_{xz} and ϵ_{xy} strains out to the eighth nearest-neighbor shell in the zinc-blende structure. The largest contributions to these numerical factors come from the nearest-neighbor shells, but there are sizeable contribu-

[27] R. M. Sternheimer, Phys. Rev. **146**, 140 (1966).

TABLE VI. Contributions to ionic field gradients.

Compound	(e/a^3) (10^{13} statcoulomb cm^{-3})	(e^*/e)[a]
InAs	2.661	+0.49
InSb	2.176	+0.46
GaAs	3.274	+0.46
GaSb	2.612	+0.43
AlSb	2.561	+0.44

[a] Reference 22.

tions from successive shells. We attach an error of $\pm 20\%$ to take into account contributions to these numerical factors from nearest-neighbor shells beyond the eighth. The ratio of V_{xy}/V_{xz} is approximately equal to $(-2.3)(\epsilon_{xy}/\epsilon_{xz})$ after the third nearest-neighbor shell. Therefore, the ionic model predicts that the ionic contribution to $S_{11}-S_{12}$ is 4.6 times the ionic contribution to S_{44} and is of opposite sign at the same nuclear position in the same compound, or

$$(S_{11}-S_{12})^i/S_{44}^i=-4.6. \tag{18}$$

The ionic model also predicts the ratio of the ionic contributions at the same nuclear positions in two different compounds. For simplicity, we assume that the antishielding coefficient is identical at the same nuclear positions in two different compounds. Using Eqs. (17) and (18), we then write, for the A nuclear positions in compounds 1 and 2,

$$\frac{(S_{11}-S_{12})^{i1}}{(S_{11}-S_{12})^{i2}}=\frac{S_{44}^{i1}}{S_{44}^{i2}}=\frac{(e_1^*/a_1^3)}{(e_2^*/a_2^3)}. \tag{19}$$

In Table VI, we give values of e/a^3 and the set of effective ionic charges computed by Coulsen, Redei, and Stocker.[23] Their paper will henceforth be referred to as CRS. The sign of the effective charge in Table VI is the sign of the A atom.

From the above development, it is apparent that the ionic point-charge model cannot alone explain the contributions to the S-tensor components given in Table IV. The relative signs of the S-tensor components measured at B nuclear positions are identical. The ionic model predicts opposite signs for the two components. The magnitudes of the measured S-tensor components can be explained by the ionic model for an effective ionic charge of 0.5 times the electron charge only by assuming antishielding coefficients much greater than 200.

TABLE VII. Values of $\langle r^{-3}\rangle$ for atomic p electrons.

Atom	$\langle r^{-3}\rangle$[a] (10^{24} cm^{-3})
Al	8.7
Ga	24
In	39
As	51
Sb	89

[a] Reference 29.

B. Covalent Model

The general form of the covalent contributions to the electric field gradient may be written[28]

$$V_{ij}\propto(1-R)(e\langle r^{-3}\rangle)(1/(1+\lambda^2)), \tag{20}$$

where $\langle r^{-3}\rangle$ is the average value of r^{-3} for the radial part of the atomic p orbital, λ is the bond ionicity, and the parameter

$$R=\langle\gamma(r)/r^3\rangle\langle r^{-3}\rangle \tag{21}$$

is coupled with the antishielding function $\gamma(r)$.[27] In Table VII we list the computed values[29] of $\langle r^{-3}\rangle$ for the atoms which occur in our samples.

We observe that the measured values of S_{44} at the B nuclear positions in InAs, InSb, GaAs, and GaSb vary from one compound to another approximately as does $\langle r^{-3}\rangle$ for the particular B atom. From Table IV, the large measured values of S_{44} are the same within experimental error at the Sb nuclear positions in InSb and GaSb, as are the values of S_{44} at the As nuclear positions in InAs and GaAs. The ratio of the experimental S_{44} at an As nuclear position to the S_{44} at an Sb nuclear position is 0.63. From Table VII, the ratio of $\langle r^{-3}\rangle$ at an As atom to $\langle r^{-3}\rangle$ at an Sb atom is 0.58. The ionic model would predict ionic contributions to S_{44} no larger than 25% of the measured value, for effective ionic charges of 0.5 times the electron charge and antishielding coefficients of 200. Therefore the variation of the measured S_{44} values at the B nuclear positions in the four compounds with the values of $\langle r^{-3}\rangle$ at the B atoms may be interpreted as indicating how the covalent contributions vary from compound to compound. From the argument presented above and from Eq. (20), we expect that λ and R will be approximately constant at the same nuclear positions in different compounds.

In the same compound at the same nuclear position, the covalent contributions to $S_{11}-S_{12}$ and S_{44} may differ only in numerical factors related to the directions of the strains. With these plausibility arguments as a basis, we assume that

$$\frac{(S_{11}-S_{12})^{c1}}{(S_{11}-S_{12})^{c2}}=\frac{S_{44}^{c1}}{S_{44}^{c2}}=K, \tag{22}$$

where K is the common ratio.

C. Separation of Ionic and Covalent Contributions

In order to apply the assumptions of the model to separate the ionic and covalent contributions to the measured S-tensor components, it is first necessary to know the ratio of the effective ionic charges at the same nuclear positions in two different compounds. We argue as does Cochran[30] that the "dynamic" effective ionic

[28] V. K. Bashenov, V. A. Presnov, and S. P. Fedotov, Phys. Status Solidi **25**, K51 (1967).
[29] R. G. Barnes and W. V. Smith, Phys. Rev. **93**, 95 (1954).
[30] W. Cochran, Nature **191**, 60 (1961).

TABLE VIII. Separated ionic and covalent contributions to the S-tensor components (in units of 10^{15} statcoulomb cm^{-3}) and covalent isotropy factors.

Compound	Nucleus	$S_{44}{}^i$	$(S_{11}-S_{12})^i$	$S_{44}{}^c$	$(S_{11}-S_{12})^c$	$\frac{2S_{44}{}^c}{(S_{11}-S_{12})^c}$
InAs	In	−6.0	27.6	−3.6	0.6	−12.0
	As	3.6	−16.5	17.6	35.6	0.99
InSb	In	−4.6	21.1	−7.1	0.9	−16.0
	Sb	6.2	−28.5	27.2	54.0	1.0
GaAs	Ga	−3.3	15.2	−6.0	−1.3	9.3
	As	4.2	−19.3	17.7	36.3	0.98
GaSb	Ga	−2.5	11.5	−8.3	−1.7	9.7
	Sb	7.1	−32.6	26.8	52.9	1.02
AlSb	Sb	5.2	−23.9	23.3	45.9	1.01

charges determined, for example, by optical experiments[31] may not be related to the effective ionic charges which create ionic electric field gradients at the nuclear position. Cochran[30] and Madelung[22] point out that only general qualitative results have been found from those experiments which might be expected to give information about ionicity and effective ionic charge. Therefore, we consider possible effective ionic charge ratios from the several sets of theoretical estimates of effective ionic charges.[23–26]

The choice among the four sets of effective ionic charges is made by determining the set agreeing best with the ordering of compounds in terms of the measured S-tensor components. From Table IV at the A nuclear positions of InAs, InSb, GaAs, and GaSb, the values of S_{44} are approximately constant and the values of $S_{11}-S_{12}$ (in units of 10^{15} statcoulomb cm^{-3}) decrease from 28 to 9.8 for the above order of compounds. Also, the isotropy factors increase at the same A nuclear positions for this same arrangement of compounds.

The ordering of compounds, InAs, InSb, GaAs, and GaSb, is in agreement with that predicted by CRS for decreasing magnitudes of positive effective ionic charge for the A atoms. Different arrangements of these four compounds for decreasing effective ionic charge are predicted by the other estimates of effective ionic charges.[24–26]

On the basis of the ionic model, it is not unreasonable to interpret the S-tensor-component behavior at the A nuclear positions in the four compounds as due to decreasing ionic contributions to the S-tensor components. The ionic model predicts that $(S_{11}-S_{12})^i$ is 4.6 times larger than $S_{44}{}^i$. Therefore, the values of the measured S_{44} could be constant while there were decreasing ionic contributions to the measured $S_{11}-S_{12}$ over the four compounds.

Using the effective ionic charge ratios from CRS, the assumptions of the model, and the magnitudes and relative signs of the S-tensor components in Table IV, we solved four equations such as those in Eqs. (16) for the following situations: for the In nuclear positions in InAs and InSb, for the Ga nuclear positions in GaAs and GaSb, for the As nuclear positions in InAs and GaAs, and the Sb nuclear positions in InSb and GaSb. The signs of the S-tensor components for different compounds relative to each other are not experimentally determined. From the solutions of the sets of four equations, we chose those signs consistent with ionic contributions whose magnitudes could be explained by antishielding coefficients of approximately 200 or less. The signs chosen are the top signs in Table IV.

For none of the sets of effective ionic charges when used with the model did the effective ionic charge of AlSb give separation of the ionic and covalent contributions consistent with InSb and GaSb contributions.

In order to separate the ionic and covalent contributions at the Sb nuclear position in AlSb, we considered the AlSb effective ionic charge to be unknown. The physical model was used to separate the ionic and covalent contributions to the S-tensor components at the Sb nuclear positions in GaSb and AlSb. However, Eq. (19) was replaced by a condition that the ionic contributions determined here for GaSb be equal to those found earlier for GaSb in analyzing InSb and GaSb. The appropriate effective ionic charge for AlSb was found to be 0.33 times the electron charge when it was referred to the CRS values for the other four compounds. With this value of effective ionic charge, the ratio of $2S_{44}{}^c/(S_{11}-S_{12})^c$ at the Sb nuclear position in AlSb is identical with the same ratios at the Sb nuclear positions in InSb and GaSb and the As nuclear positions in InAs and GaAs. In Table VIII, we present the ionic and covalent contributions to the measured S-tensor components determined from the above model and from the CRS values of effective ionic charges, except for AlSb where the value of 0.33 times the electron charge is used.

VI. CONCLUSIONS

The model that has been presented in Sec. V, used with the CRS values of effective ionic charge, allows a separation of ionic and covalent contributions to the measured S-tensor components. These separated components can now be used to give a qualitative understanding of the S-tensor components given in Table IV.

[31] M. Hass and B. W. Henvis, J. Phys. Chem. Solids 23, 1099 (1962).

(1) One dominant feature of the measured S-tensor components of all the compounds investigated is the difference in the S-tensor components at the A and B nuclear positions. The magnitudes and relative signs of $S_{11}-S_{12}$ and S_{44} and the isotropy factors at A nuclear positions are quite different from those at B nuclear positions. The results of the model given in Table VIII show that this difference may be due to the covalent contribution. The covalent isotropy factors at A nuclear positions are approximately 10 and the isotropy factors at the B nuclear positions approximately 1.0. The A-nuclear-position isotropy factors indicate that ϵ_{xy}, which are strains perpendicular to a nearest-neighbor bond direction, are less effective in producing covalent field gradients than ϵ_{xz}, the strains at an angle of 54.74° relative to a nearest-neighbor bond direction. The B-nuclear-position isotropy factors indicate that the covalent field gradients produced by equal ϵ_{xy} and ϵ_{xz} strains have the same magnitudes. The model also predicts that the signs of the covalent contributions at the B nuclear positions are positive and at the A nuclear positions they are negative or the magnitudes are small. Therefore, if covalent field gradients arise from the deformation of bonding orbitals, then the effects of the deformations and possibly the bonding orbitals are rather different when viewed from the A and B nuclear positions.

(2) The measured values of S_{44} at the B nuclear positions are two or three times larger than the measured values of S_{44} at the A nuclear positions. The model indicates that this difference may be explained by dependence of $S_{44}{}^c$ on the value of $\langle r^{-3}\rangle$ for the Sb, As, In, and Ga atoms.

(3) The measured values of $S_{11}-S_{12}$ for the four compounds InAs, InSb, GaAs, and GaSb vary much more from compound to compound at the A nuclear positions than at the B nuclear positions. From Table VIII, this different behavior of the $S_{11}-S_{12}$ tensor components may be explained by a larger covalent than ionic contribution at the B nuclear positions and a much larger ionic than covalent contribution at the A nuclear positions. The antishielding coefficients for the ionic contributions can be estimated from Table VII, the ionic model, and the effective ionic charges of CRS. These are 215 for Sb, 155 for In, 91 for As, and 76 for Ga.

(4) The measured isotropy factors at the A nuclear positions increase in the order of compounds InAs, InSb, GaAs, and GaSb. From Table VIII, this variation is explained by a decrease in the magnitude of the ionic contributions and a general increase in the covalent contributions for the above order of compounds. This is the order of the four compounds for decreasing ionicity of the chemical bond theoretically predicted by CRS and Folberth.[32]

(5) The measured value of S_{44} at the B nuclear position in AlSb is approximately 15% smaller than at the B nuclear positions in InSb and GaSb. This smaller magnitude may be explained by the model as due to a smaller effective ionic charge for AlSb and a 15% smaller covalent contribution than for the Sb nuclear positions in InSb and GaSb. The smaller covalent contribution at the Sb nuclear position in AlSb may be related to the small value of the Al $\langle r^{-3}\rangle$ as compared with the larger values of $\langle r^{-3}\rangle$ for In and Ga.

The model that we have suggested to separate ionic and covalent contributions to the measured S-tensor components does offer qualitative explanations for the behavior of the S-tensor components of Table IV. The quantitative, accurate description of the electric field gradient generation and the details of the chemical bonding require knowledge of the electronic wave functions, and particularly of the wave functions of the valence electrons.

ACKNOWLEDGMENTS

We thank Dr. Robert A. Reuhrwein of Monsanto Chemical Co. for supplying the InAs, InSb, GaAs, and GaSb single crytals. We also thank Willis Smith for checking the InSb experimental NAR data presented in this paper.

[32] O. G. Folberth, Z. Naturforsch. **13a**, 856 (1958).